Automatic Liver Vasculature Segmentation Method Using a Modified Multiscale Vesselness Filter

Marcin Rudzki, *Silesian University of Technology*

Abstract

The paper presents an automatic method for liver vasculature segmentation in volumetric images obtained during Computed Tomography (CT) patient examination. The method, apart from the CT image, also requires an additional image containing binary liver mask. A modified multiscale vesselness filter (VF) performs vasculature detection. VF response is used to determine the starting voxels for the segmentation and to calculate parameters characterizing detected blood vessels. The segmentation is done using region growing algorithm with dynamic thresholds calculated for each voxel according to the VF response. Testing was done on a set of 40 CT liver studies in portal phase. The images were of various voxel size and liver-vessels contrast. Obtained results are following: in one case the vessel tree could not be detected, in 4 cases the segmentation was of poor quality. In the remaining 35 cases the vessel tree was segmented above: 1st bifurcation (2 cases), 2nd bifurcation (11 cases) and 3rd bifurcation (22 cases).

1. Introduction

Patient preparation for liver surgery involves diagnosis with the use of tomographic imaging. Most commonly used is Computed Tomography (CT), less often Magnetic Resonance [1]. As a result a series of 2D cross-sectional images is obtained. Those images compose a single volumetric image. The value of each voxel is expressed in Hounsfield Units (HU) and results from the average X-ray attenuation factor of all tissues contained within its volume.

During a liver CT study a patient is intravenously injected with a contrast agent allowing blood vessels to be distinguished from the surrounding liver tissue. However, depending on the acquisition protocol, time, type of the contrast agent and technician's experience the achieved image contrast may vary from study to study.

From the images radiologists can perform diagnosis of the liver pathology (tumor, cirrhosis and others). During the diagnosis not only the tumor blood supply is assessed, but the vascularization of the liver is also of importance as it defines anatomical liver segments [2, 3]. Preoperative surgery planning is especially important for the minimally invasive surgical procedures, where the surgeon has much smaller field of view, thus has to know the anatomy beforehand.

Manual processing of volumetric images for vasculature delineation is time consuming and tedious due to the tree-like structure intersecting the image sections at various angles. Therefore, for years are being developed semi- or fully automatic methods for vasculature segmentation.

The paper is organized as follows: the next section describes the processing framework, with emphasis on the most important preprocessing steps, the modified vesselness filter and the segmentation algorithm. Section 3 briefly presents the testing data, in section 4 the results are described. The paper ends with a short summary in section 5.

2. Presented method

The presented method for automatic liver vasculature segmentation in CT images consists of three main stages: (1) preprocessing, (2) multiscale blood vessels detection and segmentation, (3) post processing. In all processing stages the information about voxel size obtained form DICOM [4] file header is used.

The method requires as input two volumetric images of the same size and coordinate system [4]: the image I (Fig.1) obtained during CT study and a binary mask M (Fig.2) containing segmented liver, obtained from image I by an external method. Following denotation $I_{xyz} = I(x, y, z)$ defines value of the image I at voxel located in (x, y, z).

2.1 Preprocessing

In the first step, the average v_{avg}, median v_{med} intensities and histogram h_I form the region of image I defined by the mask M are calculated. The intensity for which the histogram h_I has its maximum is found. Liver tissue intensity v_{liver} is determined by:

$$v_{liver} = \min\left(\arg\max\left(h_I(v)\right), v_{avg}, v_{med}\right). \quad (1)$$

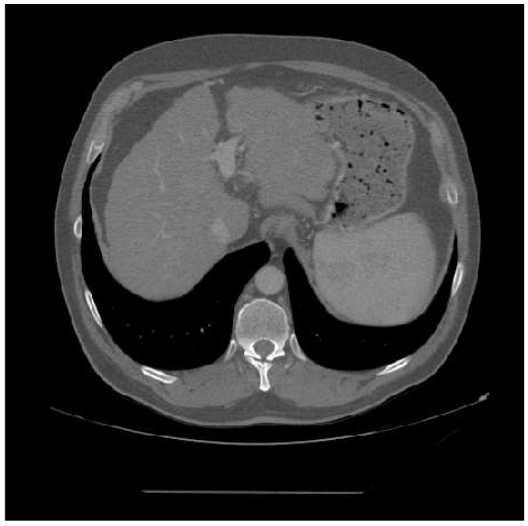

Fig.1. Transverse slice of a CT image *I*.

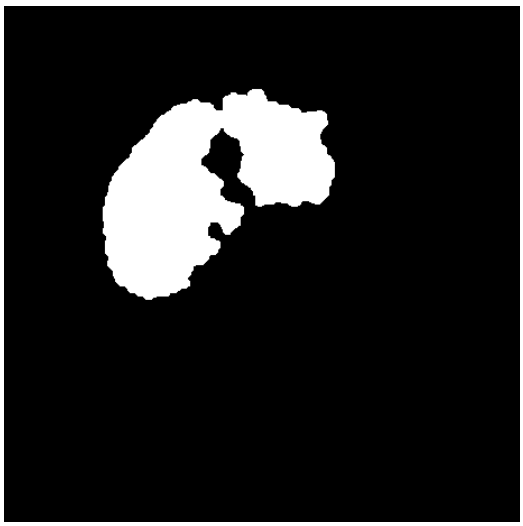

Fig.2. Corresponding slice of the mask *M*.

Obtained liver tissue intensity is used to saturate image I intensities below the value v_{liver} because none of them is of importance for vessels detection. Image I is also saturated form above at the level of 500[HU] that still allows to distinguish contrast enhanced blood vessels from bones or other hard structures

$$I_{xyz} := \begin{cases} v_{liver} & \text{if } I_{xyz} \le v_{liver} \\ I_{xyz} & \text{if } v_{liver} < I_{xyz} < 500 \\ 500 & \text{if } I_{xyz} \ge 500 \end{cases}. \quad (2)$$

Next preprocessing step required for proper vessels detection removes all structures with X-ray attenuation factor higher than the value for bone tissue (400[HU]). Such structures may be present within the liver as an erroneous operation of the external liver segmentation resulting in ribs being considered as a part of the liver or due to presence of metallic implants (Fig.3).

The procedure used for removing "hard structures" is a modified version of the one described in [5] and consists of the following steps:

1. grayscale dilation with ball structuring element of radius equal to the slice thickness;
2. region growing starting from voxels with intensity above 425[HU] and lower threshold equal to $v_{liver} + 0.25 \cdot (425 - v_{liverMax})$, where $v_{liverMax}$ is the minimal intensity for which cumulative histogram of I attains 99.9% of total counts;
3. blurring the binary result obtained in step 2 with Gaussian kernel of standard deviation 1.5 [mm];
4. subtracting image intensities according to the blurred mask as described in [5].

An example of removed metallic drain is shown in Fig.4.

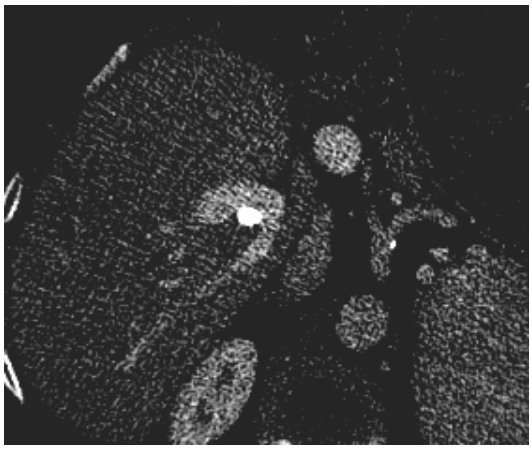

Fig.3. Metallic drain inside liver.

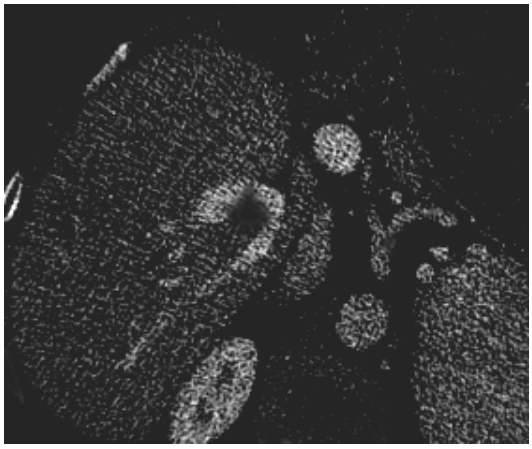

Fig.4. Metallic drain removed.

The final preprocessing step performs "soft masking" of the liver region. "Hard masking" would result in cutting largest blood vessels that are not inside the liver, but close to it, for example the portal vein (Fig.5).

"Soft masking" gradually attenuates image intensities according to (3), where d_{xyz} is the distance from voxel (x, y, z) to the nearest voxel on the liver boundary specified by mask M

$$I_{xyz} := I_{xyz} \cdot \exp\left(-\left(\frac{d_{xyz}}{15}\right)^2\right) + \\ + v_{liver} \cdot \left(1 - \exp\left(-\left(\frac{d_{xyz}}{15}\right)^2\right)\right). \quad (3)$$

This way image content that is within some margin within 3D space (here equal to 15[mm]) to the liver boundary is preserved, what can be seen in Fig.6.

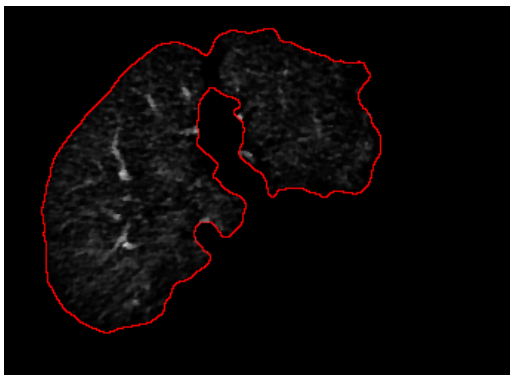

Fig.5. "Hard" masking.

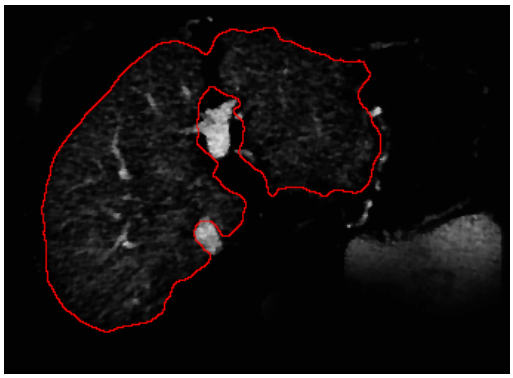

Fig.6. "Soft" masking.

2.2 Detection and segmentation

For the detection of bright vessel-like structures a modification of Frangi's vesselness filter (VF) [6] is used. Its operation employs eigen decomposition of a Hessian matrix. For each image voxel a Hessian matrix is calculated and its eigen decomposition is performed. According to the relation between the eigenvalues local image structure can be determined. The analysis within the scale-space [7, 8] uses image convolution with the derivatives of a Gaussian kernel with variance related to the scale of analysis to calculate image spatial derivatives. The multiscale analysis is repeated for several discrete values of scale and the final result is accumulated as voxel-wise maximum of the single scale responses. More detailed description of the Frangi's multiscale VF can be found in [9].

In the modified VF the response function is based on sigmoids instead of Gaussians. Also a parameter R_C was introduced after [10] that better distinguishes between plate-like, cylindrical and blob-like structures than original Frangi's parameter R_B. Following formulae define the modified VF response and all the values are calculated for every voxel (x, y, z) and scale t (subscripts omitted for clarity):

$$R_A = \frac{|\lambda_2|}{|\lambda_3|}, \quad (4)$$

$$R_C = \frac{\left|(2|\lambda_3| - |\lambda_2| - |\lambda_1|)\right|}{|\lambda_3|}, \quad (5)$$

$$v_A = \frac{1}{1 + \exp\left(-\frac{R_A - R_{Ac}}{R_{As}}\right)}, \quad (6)$$

$$v_C = \frac{1}{1 + \exp\left(-\frac{R_C - R_{Cc} + R_{Cw}}{R_{Cs}}\right)} + \\ - \frac{1}{1 + \exp\left(-\frac{R_C - R_{Cc} - R_{Cw}}{R_{Cs}}\right)}, \quad (7)$$

$$v_S = 1 - \exp\left(-\frac{S^2}{2\gamma^2}\right), \quad (8)$$

$$V_{t,xyz} = v_A \cdot v_C \cdot v_S, \quad (9)$$

where: λ_1, λ_2, λ_3 ($|\lambda_1| \le |\lambda_2| \le |\lambda_3|$) are the eigenvalues of a Hessian matrix calculated at voxel (x, y, z) and scale t, parameters R_A and R_C allow to distinguish between image structures (Tab.1).

Tab.1.

Dependence between R_A, R_C parameters and image structure

R_A	R_C	image structure
≈0	≈2	plane
≈1	≈1	tube/cylinder
≈1	≈0	sphere/*blob*

Parameter R_{Ac} defines the "center" (inflection point) of the sigmoid, R_{As} is responsible for the slope of the sigmoid. Similarly, the parameters R_{Cc}, R_{Cs} define the "center" and "slope" of the bisigmoid curve of parameter R_C, and R_{Cw} defines "half width" of the bisigmoid (Fig.7). The v_S term has exactly the same form as in the original Frangi's filter and is responsible for attenuation of the filter's response to image noise, $S = \|H_{t,xyz}\|_F$ is Frobenius matrix norm of a Hessian calculated at voxel (x, y, z) and scale t.

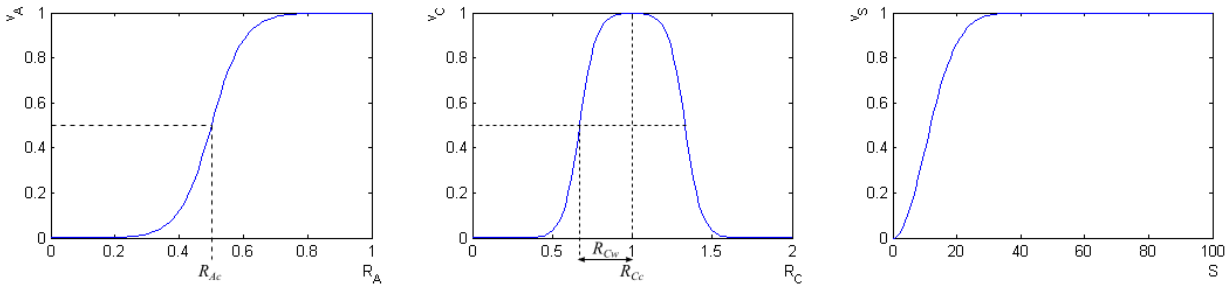

Fig.7. Response functions plots for the modified vesselness filter, R_{Ac}=0.5, R_{Cc} = 1.0, R_{As}=R_{Cs} = 0.05, R_{Cw} = 0.3, γ=10.

Automatic adaptation of the filter to image noise is possible by calculating the gamma parameter for each scale of analysis as

$$\gamma_t = \frac{\max_{xyz} \left\| H_{t,xyz} \right\|_F}{3}. \qquad (10)$$

Values of the "R" parameters are as follows: R_{Ac} = 0.5, R_{As} = 0.05, R_{Cc} = 1.0, R_{Cs} 0.05, R_{Cw} = 0.3 and follow from the theoretical relations (Tab.1). Multiscale analysis is performed for 5 discrete values of scale t corresponding to standard deviation of the Gaussian kernel form 1.5[mm] to 5.5[mm] with logarithmic spacing: $\sqrt{t}$ = {1.5; 2.07; 2.87; 3.97; 5.5}[mm].

The multiscale VF response is accumulated voxel-wise as maximum response from all scales:

$$V_{xyz} = \max_t \left(V_{t,xyz} \right). \qquad (11)$$

Resulting image V is subject to morphological dilation with spherical structuring element of radius 1 voxel (26-neighbourhood), followed by averaging using the same neighborhood. Exemplary transverse slice of the vesselness response image is shown in Fig.8.

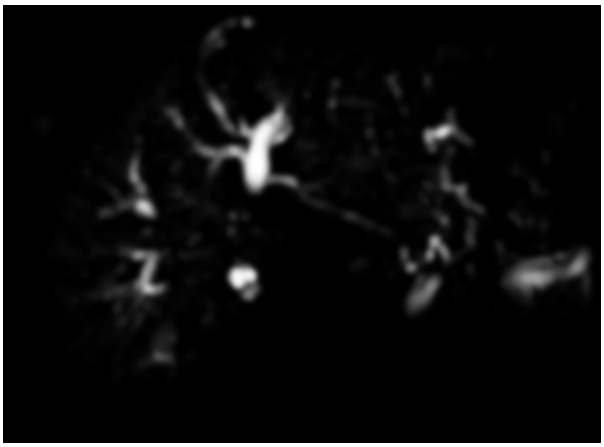

Fig.8. Image V – final response of the VF.

This image is then used to:

- determine starting points for the segmentation,
- dynamic thresholds modification during the segmentation.

Starting points are those voxels within liver for which the VF response is higher than a threshold p. The threshold is calculated form the histogram of the image V limited to the region specified as liver by the mask M. The threshold value p is determined by 10% of voxels with the highest VF response within the liver comparing to all voxels within liver with VF response higher than 0.5 (Fig.9).

Basing on the starting points the average vessel intensity v_{vess} and its standard deviation σ_{vess} are calculated. Allowed intensity range g for the segmentation is determined by

$$g = \max\left((v_{vess} - v_{liver}),\ 3\sigma_{vess} \right). \qquad (12)$$

Finally, vasculature segmentation is performed by a region growing algorithm [11] on the preprocessed image I and using auxiliary data: image V, values v_{vess} and g. Region growing iteratively adds voxels to the starting points that are 6-connected and for which the condition

$$v_{vess} - g \cdot V_{xyz} \le I_{xyz} \le v_{vess} + g \cdot V_{xyz} \qquad (13)$$

is satisfied. As a result a binary image N is obtained containing the volume of segmented liver blood vessels.

Dynamic threshold modification allows that voxels with high intensity difference, comparing to the established v_{vess} value, can be incorporated into the segmentation result as long as their spatial position is close to detected vessels spatial position by the VF. Decline of the vesselness response causes more strict condition on the allowed intensity range thus preventing from segmentation leaks even for images with relatively low liver-vessels contrast.

2.3 Postprocessing

Obtained previously image N containing the segmentation result is subject to the following postprocessing steps within 26-neighborhood:

- binary voting – if a voxel with value 1 has less than 3 neighbors with value 1, it is removed from the segmentation result, i.e. its value is changed to 0;

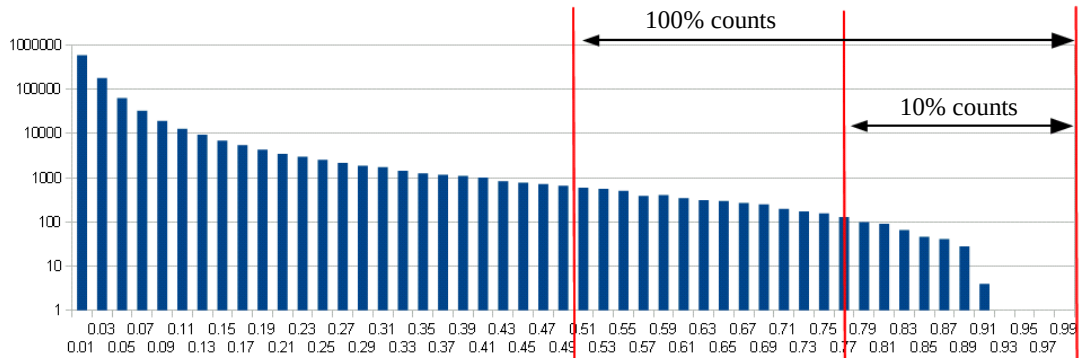

Fig.9. VF response within the liver – determination of the threshold p that defines starting points for the segmentation.

Tab.2.

Summary of the segmentation results

Quality of the segmentation	Nr of cases	Bifurcation from the portal vein	Average vessel-liver contrast[HU]	Standard deviation of the vessel-liver contrast
bad	1	0	42	-
poor	4	[1, 2)	45	18
moderate	2	[1, 2)	38	4
good	11	[2, 3)	61	20
good	22	≥3	80	35

- binary voting – if a voxel with value 0 has more than 12 voxels with value 1, it is added to the segmentation result, i.e. its value is changed to 1.

Finally, a binary median filtering of the image N also within 26-neighbourhood is performed.

Postprocessing ensures more smooth result as it removes small irregularities form the image N.

3. Testing

Testing was performed on 40 CT volumetric images of abdomen in the portal (or portal-venous) phase. The images were of various voxel size (from [0,84; 0,84; 0,62][mm] to [0,7; 0,7; 5,0][mm], most common [0,85; 0,85; 2,5][mm]). Liver–vessels contrast was also diverse, from about 35[HU] to above 150[HU]. Some of the images contained considerable CT reconstruction artifacts.

Due to lack of a "gold standard" derived form segmentation performed by experts, the assessment of the presented method performance was done only qualitatively taking into consideration number of bifurcations from the portal vein where vessels were segmented and the overall segmentation quality (leaks, discontinuities).

4. Results

The results are summarized in Table.2. In one case the vessel tree could not be detected, low liver-vessels contrast caused too low VF response to obtain starting points. In 4 cases the segmentation was of poor quality (leaks to nearby tissues, mostly heart, kidney or tumor) and in the remaining 35 cases the vessel tree was segmented above: 1st bifurcation (2 cases), 2nd bifurcation (11 cases) and 3rd bifurcation (22 cases). Exemplary 3D visualizations of the segmentation are presented in Fig.10.

5. Summary

In the article a method for automatic liver vasculature segmentation is described. The method requires two images as input (CT image and binary liver mask) and performs vessels segmentation in a completely automatic manner. The detection is based on a modified multiscale vesselness filter, in which sigmoidal response function replaces the original ones. Segmentation uses region growing algorithm with thresholds calculated dynamically for each analyzed voxel. Obtained results show the applicability of the method for vasculature segmentation in clinical CT images of various quality. In 35 out of 40 cases the vessel tree was segmented above: 1st bifurcation (2 cases), 2nd bifurcation (11 cases) and 3rd bifurcation (22 cases). Further work includes improvement of the segmentation results by involving more advanced image processing algorithms, decomposition of the vessel tree into anatomical segments that would allow automatic liver segments labeling according to Couinaud's scheme.

Acknowledgements

The images were obtained from Samodzielny Publiczny Centralny Szpital Kliniczny in Warsaw for the purpose of research grant LIDER/03/47/L-1/NCBiR/2010 founded by the Polish Center of Research and Development.

Fig.10. 3D visualization of several segmentation results.

Bibliography

[1] Prokop M., Galanski M., Van Der Molen A. J., oraz Schaefer-Prokop C., *Spiral and Multislice Computed Tomograpgy of the Body*. Thieme Medical Publishers, 2003.

[2] Couinaud C., *Liver anatomy: portal (and suprahepatic) or biliary segmentation*. Digestive surgery, vol. 16, no. 6, p. 459–467, 1999.

[3] Sylwanowicz W., Krechowiecki A., Łasiński W. and Nariewicz O., *Anatomia człowieka*. Państwowy Zakład Wydawnictw Lekarskich, 1974.

[4] National Electrical Manufacturers Association. *Digital Imaging and Communications in Medicine (DICOM)*. Online: ftp://medical.nema.org/medical/dicom/2009/

[5] Rudzki M., *Automatic image contrast enhancement method for liver vasculature detection*, 18th International Conference on Mixed Design of Integrated Circuits and Systems, p. 23, 2011.

[6] Frangi A. F., Niessen W. J., Vincken K. L., and Viergever M. A., *Multiscale vessel enhancement filtering*, Medical Image Computing and Computer Assisted Intervention MICCAI'98, p. 130-137, 1998.

[7] Lindeberg T., Scale-space theory: A basic tool for analyzing structures at different scales, Journal of Applied Statistics, p. 224_270, 1994.

[8] ter Haar Romeny B. M., *Introduction to scale-space theory: Multiscale geometric image analysis*, Utrecht University, Fourth International Conference on Visualization in Biomedical Computing, raport techn. ICU-96-21, 1996.

[9] Rudzki M., *Vessel Detection Method Based on Eigenvalues of the Hessian Matrix and its Applicability to Airway Tree Segmentation*, XI International PhD Workshop OWD 2009, Conference Archives PTETiS, Vol. 26, pp. 100-105, October 2009.

[10] Descoteaux M., Audette M. A., Chinzei K. and Siddiqi K., "*Bone Enhancement Filtering: Application to Sinus Bone Segmentation and Simulation of Pituitary Surgery*", Medical Image Computing and Computer Assisted Intervention MICCAI'2005, p. 9-16, 2005

[11] Adams R. and Bischof L., *Seeded region growing,* IEEE Transactions on Pattern Analysis and Machine Intelligence, vol. 16, nr 6, p. 641-647, 1994.

Author:

MSc. Rudzki Marcin
Silesian University of Technology
ul. Akademicka 16
44-100 Gliwice
tel. (032) 237 19 88
fax (032) 237 22 25
email: *marcin.rudzki@polsl.pl*